Rankin, A. J., Desroches, M. F., Krauskopf, B., & Lowenberg, M. H. (2010). Canard cycles in aircraft ground dynamics.

Early version, also known as pre-print

Canard cycles in aircraft ground dynamics

James Rankin, Mathieu Desroches, Bernd Krauskopf, and Mark Lowenberg
Faculty of Engineering
University of Bristol
Bristol, UK, BS8 1TR

The loss of lateral stability of an aircraft turning on the ground is associated with a rapid transition from small-amplitude oscillations to large-amplitude relaxation oscillations over a very small parameter range. This phenomenon is shown to correspond to a canard explosion, where the longitudinal velocity of the aircraft acts as a slow variable of the system. The associated family of canard cycles is identified and the canard explosion is shown to be directly related to the successive saturation of tyre forces at the two main landing gears. We present a canonical two-dimensional slow-fast vector field model that captures the key features of this type of canard explosion.

A canard explosion is one of the most striking dynamical features exhibited by systems with a separation of timescales: it describes the transition, over a minute parameter range, from small oscillations born in a Hopf bifurcation to large-scale oscillations of relaxation-type that feature slow and fast segments. Relaxation oscillations and associated canard transitions have been found in several applications, for example, in models of chemical reactions [1], neuronal activity [2] and rotating machinery [3], but the archetypal example is the Van der Pol oscillator [4]. The original treatment of canard explosion in Ref. [5] used techniques from non-standard analysis; an analytical treatment of the phenomenon followed in Ref. [6] and the first concrete example, in aircraft engine vibrations, appeared in Ref. [3].

In the Van der Pol system, as in many other examples, there is an explicit separation of timescales, meaning that the system is in a standard form with a slow variable y and a fast variable x, where the parameter ε represents the separation of timescales. The system has a cubic critical manifold for $\varepsilon = 0$ (the fast nullcline) whose outside branches are stable while its inner branch is unstable. The classical relaxation oscillations for small $\varepsilon > 0$ have two slow and two fast segments: the system slowly follows a stable branch of the critical manifold until it reaches fold point where the system jumps in the fast direction to the other stable branch. The system slowly flows to the other fold point, jumps again and the process repeats. The oscillations are actually born in a Hopf bifurcation and at the nearby transition to relaxation oscillations, which occurs in an exponentially small parameter interval, one finds a family of periodic orbits that follow a part of the unstable inner branch for a considerable length of time. Such orbits are referred to as canard orbits, hence the name canard explosion; see Refs. [5, 6] for more background information.

In this paper we present a canard explosion in a quite different context — the loss of lateral stability of a passenger aircraft making a turn on the ground under constant thrust of its engines. We consider a fully parameterized mathematical model of a midsize passenger aircraft. The aircraft has a tricycle configuration with two wing-mounted main landing gears and a nose landing gear that is used for steering. The airframe is represented with six degrees of freedom, and important nonlinear effects are captured in the component models for the tyres and the aerodynamics. The longitudinal velocity V_x, the lateral velocity V_y and the rotational velocity W_z about the vertical axis already give a reasonable description of the dynamics. Three further degrees of freedom, the vertical velocity V_z, roll velocity W_x and pitch velocity W_y need to be included in order to accurately model assymetric loading between the landing gears. This mathematical model has been validated against an industry-standard multibody dynamics model; see Ref. [7] for details. The model used here was specifically developed to work with continuation software and the results in this paper are computed using AUTO [8]. Indeed, continuation methods and bifurcation analysis [9, 10] have proved effective in the study of flight dynamics, road vehicle dynamics and aircraft ground dynamics [11–13].

Constant-radius turning circle solutions are steady-states of the model that can be tracked under variation of parameters, of which the most important one is the steering angle. We will also vary the thrust setting; all other parameters are set to realistic values as in Ref. [7]. From the application point of view, the aim is to define the safe operating limits for an aircraft turning on the ground, which corresponds to finding the parameter region where the constant-radius turning solution is stable. Beyond this stability region one finds laterally unstable behaviour where the aircraft is not able to follow the constant-radius turning solution any longer. More specifically, the stability boundary corresponds to Hopf bifurcations that give rise to stable periodic orbits, which are non-constant radius solutions [14].

Figure 1(a) shows the result of a one-parameter bifurcation analysis in the steering angle δ, where the longitudinal velocity of the aircraft V_x is used as a measure of the solutions. The engine thrust is set to $T = 14\%$ of the maximum available, a value for which laterally unstable dynamics exist [7]. The grey curve in Fig. 1(a) is a branch of steady-state solutions, which are stable along the solid segments and unstable along the dashed segment. The changes of stability occur at the Hopf bifurcations H_1 for $\delta_{H_1} \approx 2.94^\circ$ and H_2 for $\delta_{H_2} \approx 10.35^\circ$. A branch of pe-

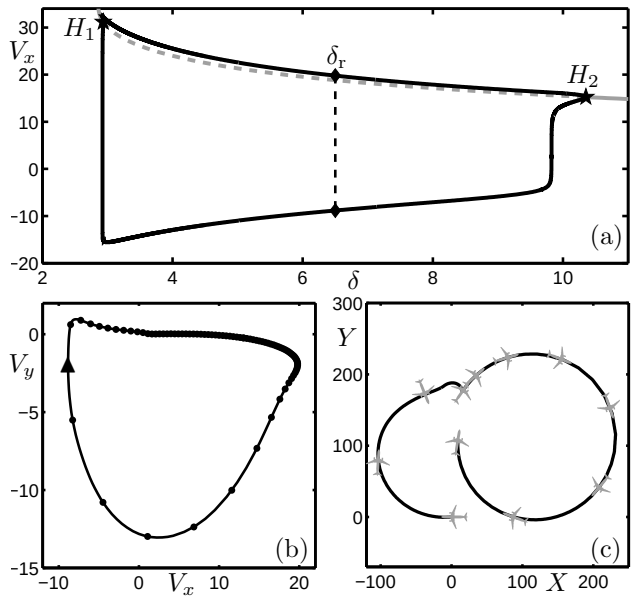

FIG. 1. Panel (a) shows a single branch (grey) of steady-state solutions represented by the longitudinal velocity V_x [m/s] as a function of the steering angle δ [deg]; the associated constant-radius turn is stable along solid grey segments and unstable along the dashed grey segment. Changes in stability occur at the Hopf points H_1 and H_2; maximal and minimal values of V_x along a connecting branch of periodic solutions are plotted in black. Panel (b) shows the (V_x, V_y)-phase plane projection of the periodic orbit at $\delta_r = 6.5°$; panel (c) shows the corresponding CG-trace in the (X, Y)-ground plane [m].

riodic solutions that connects the two Hopf bifurcations is represented in Fig. 1(a) by two black curves showing the maximal and minimal values of V_x along the branch; note that the maximal curve closely follows the unstable steady-state solutions. Near both H_1 and H_2 one notices a rapid drop in the minimal value of V_x along the periodic orbit, which then reaches a lower value that changes only gradually with δ. Figure 3(b) shows an example of a typical periodic orbit in projection onto the (V_x, V_y)-plane, namely the one at $\delta_r = 6.5°$ with a period of about 81 s. The direction of the flow along the periodic orbit is indicated by an arrow, and markers spaced at 1 s intervals indicate the slow-fast nature of the dynamics. Much more time is spent near $V_y = 0$, which indicates that V_x is a slow variable in this part of phase space; this slow part is followed by a quick transition back to small values of V_x. Overall, we find a relaxation oscillation with one slow and one fast segment, which corresponds to a laterally unstable turn. This is illustrated in Fig. 1(c) with a trace of the aircraft's center of gravity (CG) position over the (X, Y)-ground plane; markers (drawn to scale) at equally-spaced time intervals show the attitude of the aircraft relative to the CG-trace. The initial condition on the periodic orbit is chosen where the longitudinal velocity V_x is maximal. The aircraft attempts to follow a constant-radius turning circle but then starts to oversteer more and more, resulting in the loss of lateral stability and a spin; this goes along with a dramatic decrease of V_x. The aircraft then comes to a halt, after which it speeds up under the constant thrust of the engines to again attempt to follow a constant-radius turning circle and the process repeats. Note that in Fig. 1(c) it is necessary to translate and rotate a copy of the CG-trace, then align and connect it to the final point to obtain the next period's motion.

We now concentrate on the exact nature of the sharp drops in V_x near the two Hopf points. Close to H_2 the branch of periodic solutions initially grows with a square-root type progression (as is to be expected near a Hopf bifurcation); however, as δ is decreased there is a sharp and sudden drop in the minimal value of V_x at $\delta_{c2} \approx 9.83°$. Close to H_1 we find an almost immediate and even larger drop of V_x at $\delta_{c1} \approx 2.92°$. The sharp increase in the amplitude difference over a small parameter range that we find close to both Hopf bifurcations is characteristic of a canard explosion. The points of canard explosion δ_{c2} and δ_{c1} are determined here as the points on the branch of periodic orbits with steepest increase in amplitude.

We proceed to confirm that we are indeed dealing with canard explosions near H_1 and H_2. Due to the complexity of the equations of motion under consideration it is not possible to identify the timescale separation explicitly in terms of system parameters. However, we found clear evidence in Fig. 1(b) of slow-fast dynamics in the relaxation-type periodic solutions at δ_r, where V_x acts as a slow variable and V_y as a fast variable of the system. The non-trivial Floquet multipliers of the periodic orbit are all very strongly attracting ($< 10^{-6}$), and the fast variables V_z, W_x, W_y change very little. The spinning motion is captured by both the lateral velocity V_y and the rotational velocity W_z, and the former is chosen as the representative of the system's fast motion. We, therefore, present the dynamics in the (V_x, V_y)-plane and progress by computing critical manifolds — fast nullclines of the system — near H_1 and H_2. More specifically, we add the constraint $\dot{V}_x = 0$ to the system of equations, which freezes the dynamics of the slow variable V_x. By treating V_x as a parameter and computing steady states of the reduced system the critical manifolds associated the canard explosions near H_1 and H_2 can be obtained. It is important to note that, locally near the Hopf point and throughout the respective canard explosion, there is no observable dependence of the critical manifold on the steering angle δ.

Figure 2 shows the critical manifolds at δ_{c1} and δ_{c2} in panels (a) and (b), respectively; the corresponding families of periodic orbits continued from the nearby Hopf points are also shown. Each critical manifold has an upper attracting branch (solid grey curve) and a lower repelling branch (dashed grey curve). Figure 2 exhibits all the main features associated with canard cycles and a canard explosion. First of all, very close to the Hopf bifurcation H_1 and H_2 of the full system there are corresponding folds F_1 and F_2 of the critical manifold; the

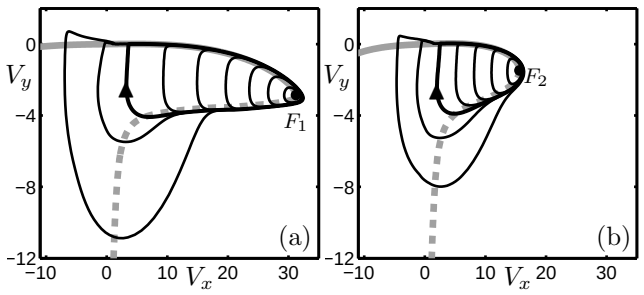

FIG. 2. Family of canard orbits in the (V_x, V_y)-plane of the canard explosion at δ_{c1} near the Hopf bifurcation H_1 (a) and at δ_{c2} near the Hopf bifurcation H_2 (b); the thick black curve indicates the maximal canard. Also shown is the critical manifold; its stable branch is solid grey and its unstable branch dashed grey.

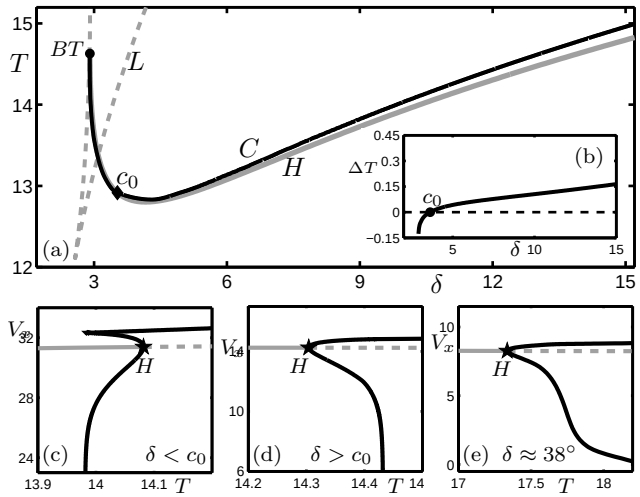

FIG. 3. Panel (a) shows a two-parameter bifurcation diagram in the (δ, T)-plane, consisting of a curve H of Hopf bifurcations (grey) and a curve L of limit point bifurcations (dashed grey) that meet at a Bogdanov-Takens bifurcation point BT; the black curve C is the locus of the canard explosion. The inset (b) shows the difference ΔT between the curves C and H as a function of δ. Panels (c), (d) and (e) show one-parameter bifurcation diagrams of V_x versus T at fixed $\delta = 2.93°$, $\delta = 12°$ and $\delta = 36°$, respectively.

distance between the Hopf and fold points is of order ε, where ε represents the timescale separation between the slow and fast variables [5]. Secondly, the periodic orbits originating from H_1 and H_2, respectively, increase rapidly in size as δ is varied away from the Hopf points. What is more, they follow not only the stable part of the critical manifold, but also a segment of its unstable branch, which clearly identifies them as canard periodic orbits. In both Fig. 2(a) and (b) we identify a maximal canard (thick black curve), which follows the unstable part of the critical manifold for the longest time. Notice further that periodic orbits that are smaller than the maximal move up from the unstable branch straight towards the stable branch of the critical manifold. By contrast, periodic orbits that are larger than the maximal canard initially move down from the unstable branch and return to the stable branch of the critical manifold after an excursion towards negative values of V_y. In the standard terminology, the smaller periodic orbits are referred to as "canards without heads" and the larger ones as "canards with heads" [5]. The canard orbits shown in Fig. 2 (a) and (b) exist over exponentially small ranges of the parameter δ. Notice that the largest periodic orbit in panel (b) is already a relaxation oscillation as it does not follow the unstable part of the critical manifold; compare with Fig. 1(b).

It is clear from Fig. 1(a) that there is a noticeable distance between the Hopf bifurcation point H_2 and the canard explosion at δ_{c2}. Near H_1, on the other hand, we find that the canard explosion at δ_{c1} occurs extremely close to H_1; moreover, the bifurcation H_1 is actually subcritical and is immediately followed by a fold of the branch of periodic orbits (although this cannot be seen on the scale of Fig. 1(a)). In order to understand this difference, we present in Fig. 3(a) a two-paramter bifurcation diagram in the (δ, T)-plane. A (solid grey) curve H of Hopf bifurcations terminates at a Bogdanov-Takens point BT on a (dashed grey) curve L of limit point (or saddle-node) bifurcations; note that the lowest point on L is a cusp point. The physical relevance of passing a limit point bifurcation in the system and the significance of the Bogdanov-Takens point are discussed in Refs. [7, 14]; we remark that the two limit points one encounters for $T = 14\%$ lie outside the range shown in Fig. 1(a). Also shown in Fig. 3(a) is the (black) curve C representing the locus of canard explosion (again determined as the point of steepest slope on the branch of periodic orbits). The curve C follows the Hopf curve H very closely for smaller values of the steering angle δ, but deviates more and more from it as δ becomes larger. In fact, the curves C and H intersect at the point $c_0 \approx (3.53°, 12.92\%)$; this can be seen clearly in the inset panel (b), which shows the signed distance ΔT in T between the two curves. We remark that the point c_0 corresponds to a degenerate Hopf bifurcation, where the branch of periodic solutions increases to full-size relaxation oscillations at the bifurcation point. Since the distance between the Hopf bifurcation H and the canard explosion C is known to be of order ε [5], Fig. 3(b) gives an indication of how ε depends on the steering angle δ (or, alternatively, on the thrust setting T). Moreover, for $\delta < c_0$ the Hopf bifurcation is subcritical as is shown in Fig. 3(c), and for $\delta > c_0$ the Hopf bifurcation is supercritical as is shown in Fig. 3(d). Note that the longitudinal velocity V_x at the Hopf point is larger in panel (c) compared with panel (d); in general, we find that $V_x \propto 1/\delta$ for solutions along H. For large values of δ the branch of periodic solutions no longer exhibits a canard explosion; rather, the transition to relaxation oscillations is gradual, as shown in Fig. 3(e).

The discussion above is crucial from an operational point of view, because it explains the type of stability

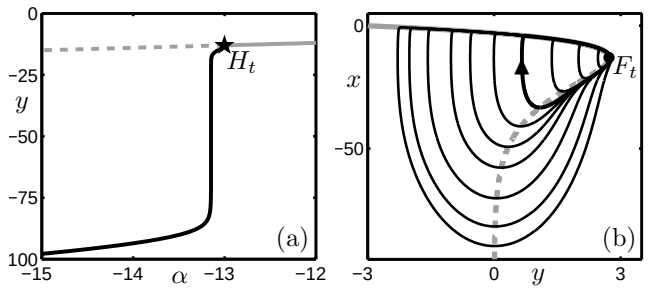

FIG. 4. Canard explosion of Eqs. (1)–(2) for $a = -3$, $b = 10$ and $\varepsilon = 0.001$. Panel (a) shows the one-parameter bifurcation diagram of y as a function of α, and panel (b) the critical manifold together with the associated canard periodic orbits in the (x, y)-plane; the maximal canard is the thicker curve with the arrow.

loss the aircraft encounters when attempting a turn with excessive speed. The subcritical case is characteristic of manoeuvres performed at high velocity, where a small steering input is sufficient for the aircraft to lose lateral stability. In this case, the forces on both the inner and the outer main landing gear tyres saturate in unison, which means that they both start to skid simultaneously. Physically, this means that the aircraft enters a spin immediately after the loss of stability of the constant-radius turn; this behaviour is represented by the dynamics following large-amplitude relaxation oscillations. In contrast, the supercritical case is characteristic of manoeuvres performed at lower velocities where a large steering input is required. In this case, when lateral stability is lost the system will initially be in the region after the Hopf point but before the canard explosion. Physically, in this dynamical regime the tyres on the inner main landing gear start to skid, but the tyres on the outer gear are still able to compensate and provide some degree of lateral stability. Hence, a complete loss of lateral stability is avoided, as long as the steering angle does not move beyond the canard explosion.

In order to capture the key qualitative features of the canard explosion found here, which differs from examples in the literature, such as the Van der Pol system, we now present the planar model vector field

$$\varepsilon \dot{x} = y + (x - a) \exp\left(\frac{x}{b}\right), \tag{1}$$

$$\dot{y} = \alpha - x, \tag{2}$$

where ε is the explicit timescale separation parameter and α is the bifurcation parameter that determines the position of the system's fixed point. The parameters a and b determine the shape of the critical manifold, which is given by setting the right-hand side of Eq. (1) equal to zero. Note the critical manifold does not depend on α; it has a fold at $x = a - b$ and the line $y = 0$ is a vertical asymptote where x tends to $-\infty$. There is a Hopf point at $\alpha = \alpha_H = a - b$, which, as is the case in the Van der Pol system, occurs exactly at the fold of the critical manifold. Figure 4 illustrates the canard explosion of Eqs. (1)–(2) for $a = -3$ and $b = 10$ and $\varepsilon = 0.001$. Panel (a) shows the characteristic steep increase in the absolute value of y after the supercritical Hopf bifurcation at $\alpha_H = -13$. The corresponding canard periodic orbits are shown in panel (b) together with the critical manifold, which has a (solid grey) stable branch and a (dashed grey) unstable branch.

Comparison of Figs. 1(a) and 2 with Fig. 4 shows that the main features of the canard explosion in the aircraft ground dynamics model have indeed been captured by Eqs. (1)–(2). Hence, this planar vector field model can be regarded as a normal form for this type of canard explosion, of which the only other example in the literature is the more complicated two-dimensional system studied in Ref. [15]. From the application's point of view, the canard cycles correspond to the rapid and total loss of lateral stability of the aircraft due to the saturation of the tyres at both main landing gears. Hence, the location of the canard explosion emerges as the most critical stability boundary from an operational and design perspective.

This research is supported by an Engineering and Physical Sciences Research Council (EPSRC) Case Award grant in collaboration with Airbus in the UK.

[1] M. Brøns and K. Bar-Eli, The Journal of Physical Chemistry **95**, 8706 (1991).
[2] J. Moehlis, Journal of Mathematical Biology **52**, 141 (2006).
[3] M. Brøns, Engineering in Industry **2**, 51 (1988).
[4] B. Van der Pol, Philosophical Magazine Series 7 **2**, 978 (1926).
[5] E. Benoît, J.-L. Callot, F. Diener, and M. Diener, Collect. Math. **32**, 37 (1981).
[6] W. Eckhaus, in *Asymptotic Analysis II*, edited by F. Verhulst (Springer-Verlag, New York, 1983), vol. **985** of *Lecture Notes in Math.*, pp. 449–494.
[7] J. Rankin, B. Krauskopf, M. Lowenberg, and E. Coetzee, ASME Journal of Computational and Nonlinear Dynamics **5** (2010).
[8] E. J. Doedel, A. R. Champneys, T. F. Fairgrieve, Y. A. Kuznetsov, B. Sandstede, and X. Wang, *Auto 97 : Continuation and bifurcation software for ordinary differential equations*, http://indy.cs.concordia.ca/auto/ (2001).
[9] B. Krauskopf, H. M. Osinga, and J. Galán-Vioque, *Numerical Continuation Methods for Dynamical Systems* (Springer, 2007).
[10] Y. A. Kuznetsov, *Elements of Applied Bifurcation Theory* (Springer-Verlag, 1998).
[11] M. H. Lowenberg, Philosophical Transactions: Mathematical, Physical and Engineering Sciences **356**, 2297

(1998), ISSN 1364503X.

[12] V. Nguyen, G. Schultz, and B. Balachandran, Journal of Computational and Nonlinear Dynamics **4**, 041007 (pages 12) (2009).

[13] P. Thota, B. Krauskopf, and M. Lowenberg, Nonlinear Dynamics **57**, 455 (2009).

[14] J. Rankin, E. Coetzee, B. Krauskopf, and M. Lowenberg, AIAA Journal of Guidance, Control, and Dynamics **32**, 499 (2009).

[15] M. Brøns, Proceedings of the Royal Society A: Mathematical, Physical and Engineering Science **461**, 2289 (2005).